Biochemistry

 Volume 41, Number 8 February 26, 2002

Articles

Mapping Proximity within Proteins Using Fluorescence Spectroscopy. A Study of T4 Lysozyme Showing That Tryptophan Residues Quench Bimane Fluorescence†

Steven E. Mansoor,‡ Hassane S. Mchaourab,§ and David L. Farrens*,‡

Departments of Biochemistry and Molecular Biology, Oregon Health & Science University, 3181 Southwest Sam Jackson Park Drive, Portland, Oregon 97201-3098, and Department of Molecular Physiology and Biophysics, Vanderbilt University, Nashville, Tennessee 37232

Received June 11, 2001; Revised Manuscript Received October 19, 2001

ABSTRACT: We present a novel method for mapping proximity within proteins. The method exploits the quenching of the fluorescent label bimane by nearby Trp residues. In studies of T4 lysozyme we show that this effect appears to be distance dependent and orientation specific. Specifically, we show that a proximal Trp residue can reduce bimane fluorescence intensity by up to 500% and induce complicated fluorescence decay kinetics. Replacing the neighboring Trp residue with phenylalanine removes these spectral perturbations. The advantages of using the Trp quenching of bimane fluorescence for protein structural studies include the low amount of protein required and the substantial simplification of labeling strategies. We anticipate this method will prove suitable for a wide array of high-throughput protein studies such as protein folding, the detection of protein−protein interactions, and, most importantly, the dynamic monitoring of conformational changes.

Site-directed labeling methods (SDL) are unique and powerful ways to study protein structure and dynamics. Generally, these methods involve introducing cysteine residues into defined regions of a protein and then attaching spectroscopic probes to the cysteines to obtain information about the local environment around each probe molecule. This approach generates an array of data from which the solvent accessibility and secondary structure of the region can be inferred (*1*−*4*).

One of these methods uses nitroxide spin labeling and EPR spectroscopy. This approach, called site-directed spin labeling (SDSL), can determine conformational changes and local secondary structure in proteins (*4*). In general, fluorescence-based strategies can be used to provide similar information (*5*−*15*).

However, the larger question of determining protein structure is a more formidable challenge with SDL methods. In addition to sequence-specific secondary structure, geometric information is required to establish the overall packing of pairs of secondary structure elements. With the spin labeling method, this problem can be overcome by measuring spin−spin interactions between two nitroxide spin labels (*16*−*20*).

Fluorescence-based SDL strategies for measuring distances are not as straightforward. The classical approach has been to measure fluorescence resonance energy transfer (FRET) between two fluorescent probes on different parts of the protein (*12*−*14*). Although powerful, the FRET approach is usually complicated by the need to label with two different, spectrally overlapping probes and by the orientation factor

† This work was supported by Grants EY12095 to D.L.F. and EY12018 and EY12683 to H.S.M. from the National Eye Institute.

* To whom correspondence should be addressed. Telephone: (503) 494-0583. Fax: (503) 494-8393. E-mail: farrensd@ohsu.edu.

‡ Oregon Health & Science University.

§ Vanderbilt University.

10.1021/bi011198i CCC: $22.00
Published on Web 02/19/2002

required for data analysis. Also, the linear range of distances that can be determined by FRET (usually 30−70 Å) is often too large to be useful for determining very close packing between secondary structure elements in proteins, since the size of the probes often used is larger than 10 Å.

We report in this paper a new, simple way to obtain short-range distance constraints in proteins by fluorescence spectroscopy. Conceptually, our approach is similar to recent methods which selectively introduce fluorescence quenching groups into proteins (*21*, *22*). The method we describe here exploits the ability of tryptophan to quench the fluorescence of the cysteine-specific probe, bimane. Because this approach eliminates the need for the use of two different fluorescent probes and operates over much shorter ranges (essentially collision or contact distance), it complements the longer range FRET methods for protein structure and dynamics studies. Furthermore, because the Trp quencher is built into the protein sequence, the labeling strategies are substantially simplified.

We recently deduced that Trp quenches bimane fluorescence upon further analysis of our previous SDFL work on T4 lysozyme (T4L)[1] (*9*). In that work we found that bimane fluorescence was unusually low at several sites on the protein and showed complicated decay kinetics. Intriguingly, the location of these sites did not follow any obvious pattern with respect to their topological or secondary structure location.

Upon closer examination of the crystal structure of T4L, we noticed that these anomalous sites are within ~6 Å of one of the Trp residues in the native protein, as illustrated in Figure 1. Four of the sites, 121, 124, 129, and 133, showed abnormally low fluorescence quantum yields, as well as complex fluorescence decays (see Figure 4 in ref *9*). We hypothesized that these Trp residues may be interacting with and influencing the fluorescence properties of neighboring bimane residues. The physical basis of this effect has previously been established by Kosower and colleagues, who found that Trp strongly quenches the fluorescence of bimane free in solution and when attached to small peptides (3−4 amino acids in length) (*23*).

In this paper we present results showing that proximal Trp residues cause quenching of bimane in proteins, thus explaining the unusual fluorescence observed in our previous work (*9*). Further, we show that this property is distance-dependent and can be used to map distances between Trp and bimane probes introduced at strategic sites in a protein. We discuss future uses of Trp/bimane quenching for SDFL studies in the context of protein fold determination, detection of protein−protein interactions, and resolving protein conformational changes.

MATERIALS AND METHODS

Materials. The reagents (fluorescent label, etc.) and the equipment (filters, cuvettes, etc.) used were identical to those described previously (*9*). The cysteine-free pseudo-wild-type lysozyme gene containing the substitutions C54T and C97A

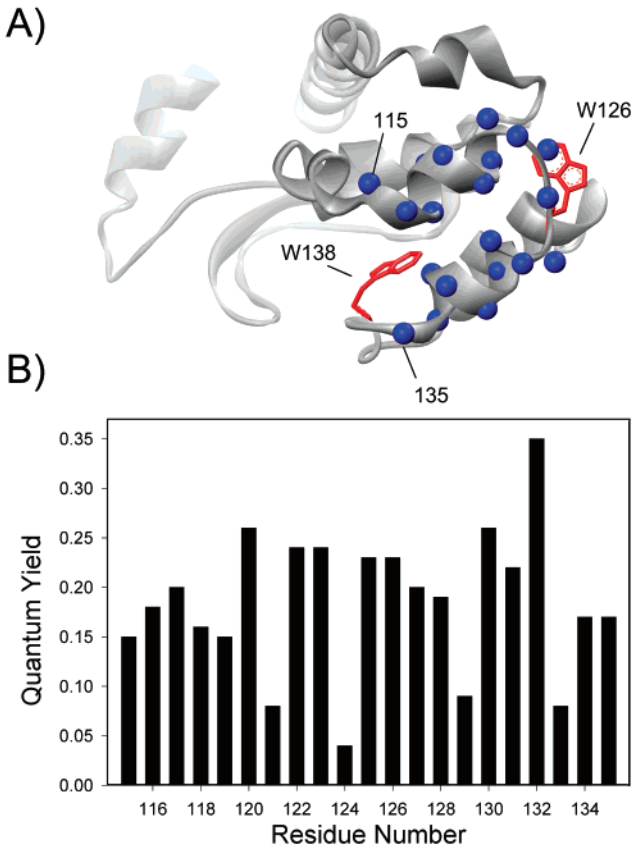

FIGURE 1: (A) Model of T4 lysozyme based on the crystal structure. The model indicates the location of two of the Trp residues in T4 lysozyme, as well as the α-carbons for the 21 cysteine substitutions labeled with monobromobimane described previously (*9*). (B) Relative quantum yields of mBBr labels attached to the 21 cysteine sites. Notice that sites 121, 124, 129, and 133 all show dramatically lower quantum yields. These residues also lay close to the two Trp residues shown in (A) above.

(*24*, *25*) was kindly provided by F. W. Dahlquist (University of Oregon). Hereafter, this mutant will be called the "wild type" or T4L.

The buffers used were as follows: buffer A, 50 mM MOPS, 50 mM Tris, and 1 mM EDTA, pH 7.6; buffer B, 20 mM Tris, 20 mM MOPS, 0.02% sodium azide, 1 mM EDTA, and 1 mM DTT, pH 7.6; buffer C, 20 mM KH_2PO_4 and 25 mM KCl, pH 3.0; buffer D, 50 mM MOPS, 50 mM Tris, 1 mM EDTA, pH 7.6, and 3 M guanidine hydrochloride.

Construction of T4L Mutants. Site-directed mutagenesis was carried out using polymerase chain reaction (PCR) methods (*26*). To facilitate this work, two new restriction sites, *Sph*I and *Xba*I, were introduced into the previously described plasmid using the overlap extension method. Oligonucleotides containing the X to cysteine substitution and overlapping either of the restriction sites were used to generate PCR fragments. The PCR fragments were then digested and ligated into the appropriate cloning vector, and the mutant constructs were confirmed by DNA sequencing.

Nomenclature. Throughout this paper, mutants are named by specifying the original residue, the number of the residue, and the new residue, in that order. For example, the code K124C indicates that the native lysine residue at the 124th amino acid position was mutated to a cysteine. Similarly, N116W indicates the native asparagine was mutated to a

[1] Abbreviations: mBBr, monobromobimane; MOPS, 3-(*N*-morpholino)-propanesulfonic acid; EDTA, *N*,*N*′-1,2-ethanediylbis[*N*-(carboxymethyl)glycine] disodium salt; Tris, 2-amino-2-(hydroxymethyl)-1,3-propanediol; T4L, T4 lysozyme; Trp, tryptophan; PET, photoinduced electron transfer; Phe, phenylalanine; SCE, standard calomel electrode; IPTG, isopropyl β-thiogalactoside.

tryptophan. Mutants labeled with mBBr are named by specifying the original residue, the number of the residue, and the suffix B_1, indicating the monobromobimane label. For example, the code $K124B_1$ indicates that the native lysine residue at the 124th amino acid position has been mutated to a cysteine and reacted with the mBBr label.

Expression and Purification of T4L Mutants. Expression of mutant proteins was as described previously (*9*, *27*). Briefly, K38 *Escherichia coli* cells were transformed with the T4L cysteine mutant plasmid (*28*), and protein production was induced in log phase cultures ($OD_{595nm} = 1.2$). After 90−120 min of shaking at room temperature, the cells were harvested, and the cell pellet was resuspended in 30 mL of buffer B, lysed, and clarified by centrifugation followed by filtration. DTT was added to the filtered cell solution to 20 mM, and after 30 min, the solution was loaded onto a cation-exchange column (Pharmacia Biotech HiTrap, 1 mL SP) equilibrated with buffer A. The samples were eluted with an increasing salt gradient from 0 to 1 M NaCl. The purity of the proteins was assessed by SDS−PAGE and judged to be at least 90% pure for all samples studied.

Fluorescence Labeling of T4L Mutants. Labeling of each lysozyme mutant was carried out by using a 10× molar excess of the fluorescent label in buffer D at 4 °C overnight. Free label was separated from the labeled protein by gel filtration on a desalting column (Pharmacia Biotech HiTrap, 5 mL) equilibrated with buffer A. Absorption spectra (measured using a Shimadzu UV 1601) were used to calculate the labeling efficiency for each mutant. Concentrations were calculated using extinction coefficients of $\epsilon_{280} = 23327$ L cm^{-1} mol^{-1} for T4 lysozyme and $\epsilon_{380} = 5000$ L cm^{-1} mol^{-1} for mBBr. To correct for mutants in which a Trp residue was either introduced or removed, an extinction coefficient value of $\epsilon_{280} = 5600$ L cm^{-1} mol^{-1} was either added or subtracted to the WT T4 lysozyme extinction coefficient. (Note that a mutation from a tryptophan to a phenylalanine resulted in an extinction coefficient of $\epsilon_{280} = 18027$ L cm^{-1} mol^{-1}.) The contribution from mBBr at 280 nm was subtracted before the protein concentrations were calculated. Control experiments using the cysteine-less WT protein showed that background labeling was less than 3% (as judged by absorption and fluorescence spectroscopy).

Thermodynamic Stability. Analysis of thermal unfolding properties was used to assess the stability of each mBBr-labeled mutant (*29*, *30*). This analysis was carried out by monitoring the tryptophan fluorescence emission intensity at 320 and 350 nm as a function of temperature (*9*). At the point of thermal denaturation, the emission intensities at each of these wavelengths change due to the solvent-sensitive property of tryptophan fluorescence (*29*, *31*).

The details of the measurements were as previously described (*9*). Briefly, 2 μM labeled protein (dialyzed against buffer C) were measured using the PTI steady-state fluorescence spectrophotometer in a T-format. Samples were excited at 280 nm and monitored at 350 and 320 nm. The melts involved ramping the temperature from 6 to 80 °C at a rate of 2°/min, after which the samples were cooled to 6 °C, to determine the extent of protein refolding, and melted again. The mutants showed greater than 75% refolding, as judged by the extent to which the ratio returned to its starting value (except $L133B_1$/W138F). The melts were done in duplicate, and the reported T_m values are the average of the two melts. Analysis of the thermal melt data was performed assuming an equilibrium of a two-state model (native folded state and totally denatured state) (*29*, *30*).

With the assumptions made by Becktel and Schellman that $\Delta S_{mutant} \cong \Delta S_{wt}$ (*32*), $\Delta\Delta G$ values for each mBBr-labeled T4 lysozyme mutant were calculated using the approximation:

$$\Delta\Delta G = \Delta T_m \Delta S_{wt}$$

where ΔT_m is the difference in melting temperatures between the mutant and the wild type and the ΔS_{wt} value is the change in entropy between the folded and denatured states of the wild-type protein. For more details, see refs *9* and *32*.

Steady-State Fluorescence. Unless noted otherwise, the steady-state fluorescence measurements of mBBr-labeled mutants were carried out at 22 °C, using 2 μM to 10 μM sample in buffer A and the PTI fluorometer. The fluorescence emission spectra were measured from 395 to 600 nm (1 nm slits) while being excited at 381 nm (2 nm slits).

Quantum Yield Measurements. The quantum yield for each mBBr-labeled mutant was measured as described previously (*9*) using quinine sulfate (quantum yield equal to 0.55 in 1 N H_2SO_4) as the standard. Emission spectra were taken using 360 nm excitation (3 nm slit width) from 370 to 700 nm (1 nm slits). Measurements were at 22° C using ∼2 μM to 10 μM bimane-labeled lysozyme mutants and for the quinine sulfate standard.

Fluorescence Lifetime Measurements. The fluorescence lifetimes of the mBBr mutants were measured as previously described (*9*). Briefly, the measurements were carried out at 22 °C using a PTI Laserstrobe fluorescence lifetime instrument on 250 μL of a 2−10 μM sample placed in a 4 mm black-jacketed cuvette. The samples were excited at 381 nm (pulses of fwhm ∼1.5 ns), and fluorescence emission was monitored through two long-pass filters (>470 nm). Each data point on a lifetime decay curve represents two averages of five laser flashes, and each decay represents 150 of these data points spaced out over the collection time interval.

Data were acquired using an arithmetic data collection method and analyzed using the commercial PTI software. Both the exponential series method (ESM) and a two-exponential decay model were used in the analysis (*33*−*35*). In brief, the ESM analysis fits the decay data using a series of exponentials with fixed, logarithmically spaced lifetimes and variable preexponentials. In the present ESM analysis, the fluorescence decays were fit allowing 100 discrete lifetimes of varying amplitude from 0.1 to 30 ns until the χ^2 value was minimized. Plots of ESM analysis are included because they provide a graphical way to differentiate between continuous lifetime distributions and discrete, multiexponential decays. Thus, analysis of the ESM plots provides a rapid way to qualitatively assess the proximity between a bimane label and a Trp residue. The decay data were also fit to a two-exponential decay model, and these values were used to calculate weighted lifetime values.

Calculation of the Driving Force for Photoinduced Electron Transfer Rates (PET). The driving force (ΔG_{el}) for the PET was calculated using a form of the Rehm−Weller equation (*36*−*38*):

$$\Delta G_{el} = e[E_{ox}(D) - E_{red}(A)] - \Delta G_{oo} - w_p$$

Table 1: Characterization of Bimane-Labeled Mutants

mutant	mol of label/ mol of T4L[a]	ΔT_m[b,c] (°C)	$\Delta\Delta G$[b,c] (kcal/mol)	abs λ_{max}[e] (nm)	em λ_{max} (nm)	quantum yield[f] (Φ)
$K124B_1$	0.9	-2.5 ± 0.2[c]	-0.7[c]	392	472.4 ± 0.6	0.036 ± 0.005
$K124B_1$/W126F	0.9	-4.0 ± 0.3	-1.2	391	472.3 ± 0.1	0.185 ± 0.009
$L133B_1$	1.2	-19.5 ± 1.0[c]	-5.5[c]	380	456.9 ± 0.6	0.096 ± 0.016
$L133B_1$/W138F	1.0	-20.4 ± 1.0	-6.0[d]	382	452.3 ± 2.8	0.573 ± 0.017
$D72B_1$	0.9	-0.9 ± 0.1	-0.3	385	463.8 ± 0.4	0.294 ± 0.043
$D72B_1$/R76W	1.1	-2.1 ± 0.2	-0.6	387	465.3 ± 0.5	0.057 ± 0.006
$Q123B_1$	0.9	$+0.3 \pm 0.5$[c]	$+0.1$[c]	388	468.9 ± 0.4	0.220 ± 0.017
N116W/$Q123B_1$	1.0	-4.0 ± 0.3	-1.2	390	469.1 ± 0.8	0.135 ± 0.004
$E128B_1$	1.0	-1.8 ± 0.3[c]	-0.5[c]	401	469.5 ± 0.5	0.182 ± 0.001
N116W/$E128B_1$	1.0	-7.0 ± 0.5	-2.1	397	469.7 ± 0.5	0.043 ± 0.003
$N132B_1$	0.9	$+1.8 \pm 0.2$[c]	$+0.5$[c]	386	466.8 ± 0.1	0.201 ± 0.004
N116W/$N132B_1$	0.9	$+3.1 \pm 0.8$	$+0.9$	394	468.9 ± 0.4	0.047 ± 0.004
$K135B_1$	0.9	-0.6 ± 0.2[c]	-0.2[c]	391	472.0 ± 0.7	0.146 ± 0.023
N116W/$K135B_1$	1.0	-4.0 ± 0.2	-1.2	390	471.0 ± 0.3	0.118 ± 0.022

[a] Represents an average of two independent labeling experiments; the standard error of the mean on all mutants $<\pm 0.1$. [b] Values are in comparison to wild-type lysozyme, $T_m = 53.0$ °C and $\Delta S_{wt} = 292.8$ cal·mol^{-1} K^{-1}; $\Delta\Delta G$ calculated using the approximation that $\Delta\Delta G = \Delta T_m \Delta S_{wt}$. [c] ΔT_m and $\Delta\Delta G$ values for the indicated mutants are from ref *9* and are provided for comparison purposes. [d] Apparent $\Delta\Delta G$ value as this mutant did not appear to be fully reversible. [e] Represents an average of two values; all values have a standard error of $<\pm 1$ nm. [f] Quantum yields were measured by integrating fluorescence intensity from 370 to 700 nm with 360 nm excitation using quinine sulfate in 1 N H_2SO_4 as the standard.

The above variables are defined as follows: e is the conversion factor from eV to kcal/mol (1 eV = 23.061 kcal/mol). E_{ox} and E_{red} are the donor (D, Trp) and acceptor (A, bimane) redox values [$E_{red} = -1.38$ V vs SCE for bimane (*39*) and $E_{ox} = 1.00$ V vs SCE for Trp (*40*)]. The ΔG_{oo} term is the energy for the bimane excited state (at 381 nm ΔG_{oo} = 75 kcal/mol, or 3.25 eV). Finally, the w_p term represents the "work" term for the Coulombic attraction felt by the transiently charged species. For the present work we approximated $w_p = -1.3$ kcal/mol assuming a center to center distance between the bimane and Trp of 7 Å (*38*). Using the above relationships, the driving force for the electron transfer was calculated to be $\Delta G_{el} = -18.8$ kcal/mol (or -0.816 eV), suggesting an exergonic photoinduced electron transfer.

Calculation of Photoinduced Electron Transfer Rates (PET). Electron transfer rates were calculated from the weighted fluorescence lifetimes [$\langle\tau\rangle = f_1\tau_1 + f_2\tau_2$, where $f_1 = \alpha_1/(\alpha_1 + \alpha_2)$ and $f_2 = \alpha_2/(\alpha_1 + \alpha_2)$] by using the relationship $k_{ET}^{\tau} = 1/\tau - 1/\tau_{ref}$ (*41*). In this analysis, the lifetime of the bimane-labeled sample in the presence of the proximal Trp residue (τ_w) was used for τ, and the lifetime of the samples lacking the Trp residue (τ_0) was used for τ_{ref}. Similarly, the steady-state fluorescence data were used to calculate electron-transfer rates using the relationship $k_{ET}^{F} = (F_0/F_w - 1)/\tau_0$, where F_w and F_0 represent the integrated fluorescence intensity (from 410 to 600 nm, with excitation at 381 nm) of the bimane-labeled samples with and without the proximal Trp residue, respectively. τ_0 represents the lifetime value as defined above.

RESULTS

Construction and Characterization of Mutants $K124B_1$/W126F and $L133B_1$/W138F. As discussed in the introduction, a prior SDFL scan of T4 lysozyme showed perturbed fluorescence from bimane labels at several sites on the protein, especially sites 124 and 133 (see Figures 1 and 4 in ref *9*). To determine if these perturbations were due to neighboring tryptophan residues, we substituted the "suspect" neighboring Trp residues to phenylalanines (W126F to test site 124 and W138F to test site 133). Both mutants could incorporate the bimane label with similar efficiency (Table 1). Neither Trp substitution resulted in a dramatic destabilization of the bimane-labeled cysteine mutant protein beyond that reported previously, indicating the overall fold of the protein was not significantly altered (Table 1) (*42*). The ΔT_m and $\Delta\Delta G$ values for mutants $L133B_1$ and $L133B_1$/W138F are larger than the values for the other mutants. However, such a result is not unexpected and, in fact, would be predicted. Residue 133 is the most buried (least solvent exposed) of the residues in the present study, and it has been previously found that destabilization is larger for substitutions at completely buried sites (*9*, *42*). Thus, because mutations at site 133 result in large $\Delta\Delta G$ values, it is possible that both mutants $L133B_1$ and $L133B_1$/W138F contain a small fraction of sample that is not fully folded under the experimental conditions. Note that, for all of the data reported below, the samples were matched, by absorbance, to have the same bimane concentration during the measurements.

Mutating the Neighboring Tryptophan Residue to Phenylalanine Causes an Increase in Bimane Fluorescence Intensity and Lifetime at Sites 124 and 133. Figures 2 and 3 show the results of making the W126F and W138F substitutions on the fluorescence of bimane labels attached to sites K124C and L133C, respectively. Figure 2A shows the location of K124 and W126 on the T4L structure. Figure 2B and Table 1 show how the fluorescence increases approximately 5-fold upon the W126F mutation, with a concomitant increase in the fluorescence lifetime (Figure 2C, Table 2). Simplification of the decay kinetics is also seen, as reflected in the two-exponential (Table 2) and ESM analysis (Figure 2D). Similarly, the W → F mutation at site 138 (Figure 3A) results in an approximate 5-fold increase in fluorescence intensity (quantum yield) from the bimane label at site 133 (Figure 3B, Table 1). The W138F mutation also results in an increased fluorescence lifetime (Figure 3C, Table 2) and simplified decay kinetics in the ESM analysis (Figure 3D). Interestingly, for both mutants, removing the neighboring tryptophan changes the complicated lifetime distribution (Figures 2D and 3D, top half) to essentially one lifetime (Figures 2D and 3D, bottom half).

With the exception of position 133, an overlap of the (normalized) fluorescence emission spectrum from each

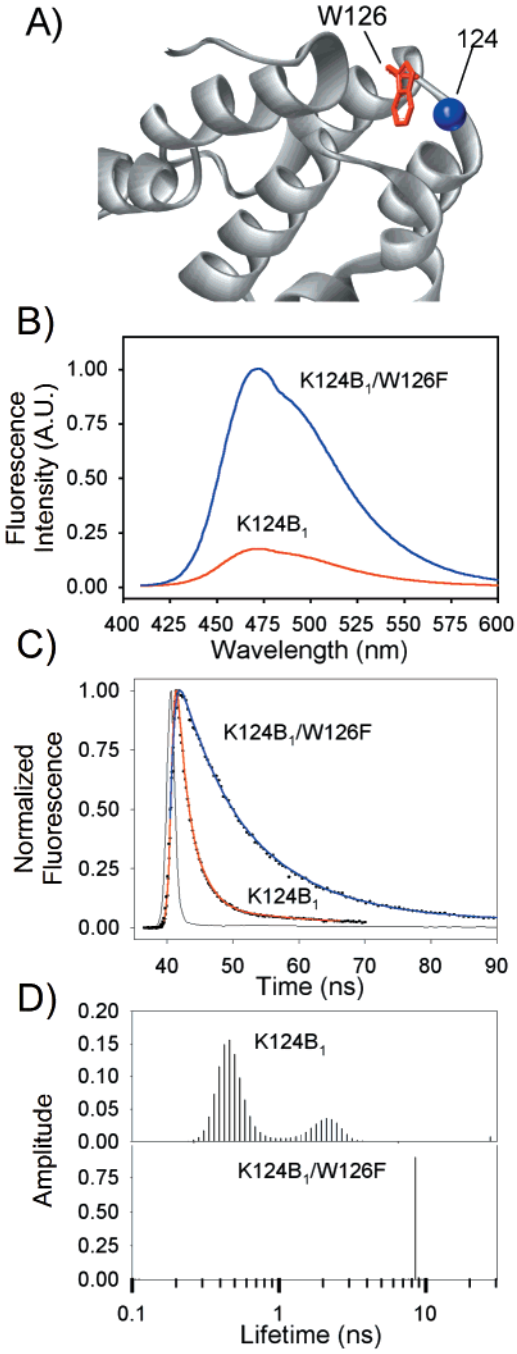

FIGURE 2: Location and fluorescence properties of bimane labels at site 124 before and after mutating the neighboring Trp residue at site 126. (A) Model of T4 lysozyme indicating α-carbon for site $K124B_1$ and W126. (B) Fluorescence emission spectrum of $K124B_1$ and $K124B_1$/W126F. Notice the ~5× difference in fluorescence intensity between the samples, even though the samples contained identical amounts of bimane label. (C) Fluorescence decay of $K124B_1$ and $K124B_1$/W126F. (D) ESM analysis of mutants $K124B_1$ and $K124B_1$/W126F. Notice that the complex ESM pattern observed for the sample containing the neighboring Trp residue is replaced by a pattern showing only one apparent lifetime upon converting the Trp residues to Phe.

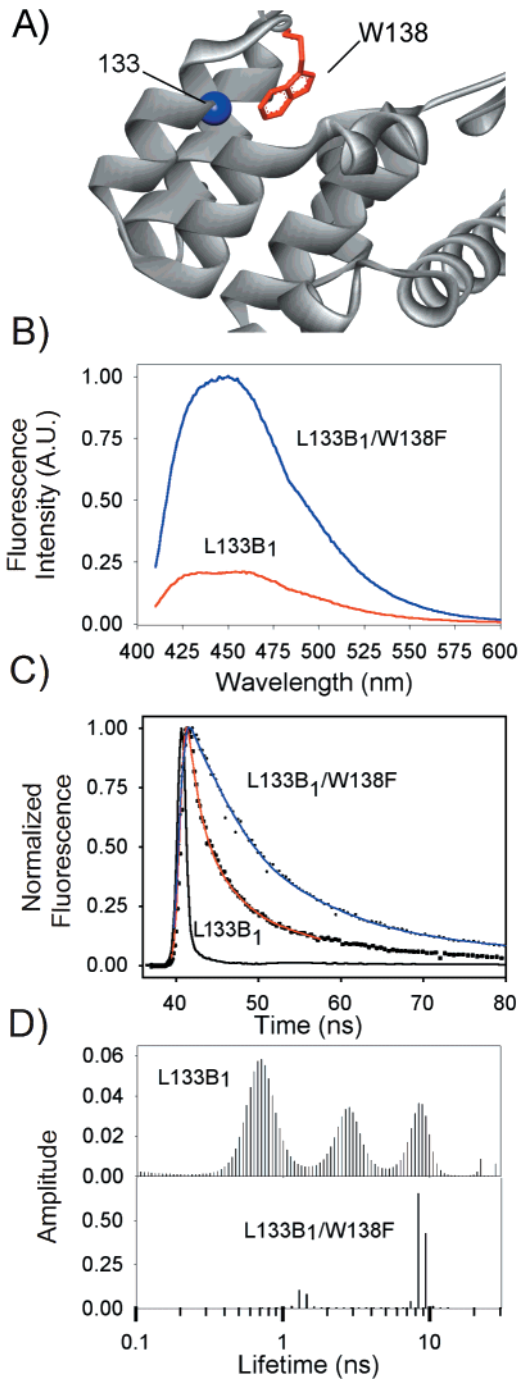

FIGURE 3: Location and fluorescence properties of bimane labels at site 133 before and after mutating the neighboring Trp residue at site 138. (A) Model of T4 lysozyme indicating α-carbon for site $L133B_1$ and W138. (B) Fluorescence emission spectrum of $L133B_1$ and $L133B_1$/W138F. Notice the ~5× difference in fluorescence intensity between the samples containing identical amounts of bimane label. (C) Fluorescence decay of $L133B_1$ and $L133B_1$/W138F. (D) ESM analysis of mutants $L133B_1$ and $L133B_1$/W138F. Notice that the complex ESM pattern observed for the sample containing the neighboring Trp residue is replaced by a pattern showing only a low number of apparent lifetimes upon converting the Trp residues to Phe.

sample demonstrates that the λ_{max} of fluorescence emission does not show significant changes due to the Trp → Phe substitution (Table 1). This latter result indicates that the difference in intensity is not due to a repacking/change in hydrophobicity of the bimane label.

Construction and Characterization of Mutants $D72B_1$ and $D72B_1$/R76W. To investigate if a Trp can be introduced to alter the fluorescence of a neighboring bimane residue, we introduced a Trp at site 76, one turn away from a bimane label attached at site 72. We chose this pair of sites because the 72/76 pair is on the exposed surface of the long helix in T4L and substitutions are unlikely to disturb the structure (Figure 4A). Furthermore, the $i + 4$ residue where the Trp

Table 2: Two-Exponential Lifetime Analysis of the Fluorescence Decay Measurements[a]

mutant	τ_1 (ns)	f_1	τ_2 (ns)	f_2	χ^2	$\langle\tau\rangle^b$ (ns)
$K124B_1$	4.9	0.2	1.4	0.8	1.0	2.1 ± 1.3e−2
	4.4	0.2	1.3	0.8	1.0	
$K124B_1/W126F$	9.5	1.0			1.1	9.4 ± 3.8e−2
	9.4	1.0			0.9	
$L133B_1$	7.0	0.3	1.0	0.7	1.0	3.1 ± 0.1
	7.2	0.3	1.3	0.7	1.4	
$L133B_1/W138F$	8.6	0.7	0.7	0.3	1.1	6.8 ± 0.2
	8.9	0.8	0.9	0.2	1.0	
$D72B_1$	9.7	1.0			0.9	9.8 ± 0.1
	9.9	1.0			1.0	
$D72B_1/R76W$	6.6	0.5	0.7	0.5	0.7	4.1 ± 0.1
	6.6	0.6	0.9	0.4	1.0	
$Q123B_1$	9.8	1.0	2.4e−3	1.9e−2	1.1	8.9 ± 0.4
	9.9	0.8	2.2e−2	0.2	1.4	
$N116W/Q123B_1$	7.2	0.7	0.5	0.3	1.1	5.6 ± 0.3
	7.4	0.8	1.0	0.2	0.8	
$E128B_1$	8.7	1.0	0.9	4.5e−3	0.8	8.5 ± 0.1
	8.7	0.9	0.8	0.1	0.9	
$N116W/E128B_1$	4.9	0.3	0.9	0.7	0.9	2.1 ± 6.9e−3
	4.9	0.3	0.9	0.7	0.9	
$N132B_1$	11.8	0.9	0.3	0.1	1.0	10.9 ± 0.4
	12.3	0.9	1.2	0.1	0.9	
$N116W/N132B_1$	8.3	0.6	0.7	0.4	0.8	6.2 ± 0.6
	9.4	0.7	2.1	0.3	0.9	
$K135B_1$	8.9	0.6	0.6	0.4	0.7	6.5 ± 0.3
	8.7	0.8	1.1	0.2	0.9	
$N116W/K135B_1$	6.0	0.8	0.7	0.2	1.0	4.8 ± 3.2e−2
	6.1	0.7	0.7	0.3	0.8	

[a] Excitation wavelength 381 nm; emission collected using two >470 nm long-pass filters. Two sets of the lifetime data are reported for comparison purposes. Abbreviations: τ_1, τ_2, fluorescence lifetimes in nanoseconds; f_1, f_2, fractional amplitude of each lifetime; $f_1 = \alpha_1/\sum\alpha_i$ and $f_2 = \alpha_2/\sum\alpha_i$, where α_1 and α_2 are the preexponential factors for τ_1 and τ_2, respectively; χ^2, chi-squared value of the fit. [b] $\langle\tau\rangle = f_1\tau_1 + f_2\tau_2$, the lifetime weighted quantum yield. The $\langle\tau\rangle$ values represent the average of the two reported sets of lifetimes ± the standard error of the mean.

is introduced is located away from termini, allowing a better estimation of the distance separation between the Trp and the bimane side chains. Both mutants could be labeled with bimane to unity. Neither the introduction and labeling of the cysteine residue at site 72 nor the $D72B_1/R76W$ mutation had much effect on the thermodynamic properties of the protein (Table 1).

Introducing the Trp at site 76 caused a dramatic decrease in intensity (Figure 4B, Table 1) and shortened and complicated the fluorescence decay properties (Figure 4C,D, Table 2).

Construction of N116W Mutants To Measure Distance Dependencies of Bimane Quenching by Trp. We next tested if tryptophan quenching of bimane can be used to obtain proximity information between secondary structure elements in proteins. A reference Trp was introduced at site 116 at the N-terminus of helix G, and the bimane probe was introduced on selected surface-exposed residues on helix H, a neighboring helix in the structure. The location of the mutation, N116W, and the four sites are shown in Figure 5A. The neighboring bimane attachment sites predicted to be potentially affected by the Trp residue (sites 123, 128, 132, 135) are in various distances from this Trp site. The sites encompass an $i + 8$ as well as several different interhelix distances, thus allowing for a qualitative assessment of the distance dependence of the Trp → bimane quenching phenomena. The Trp substitutions at N116 did not appear

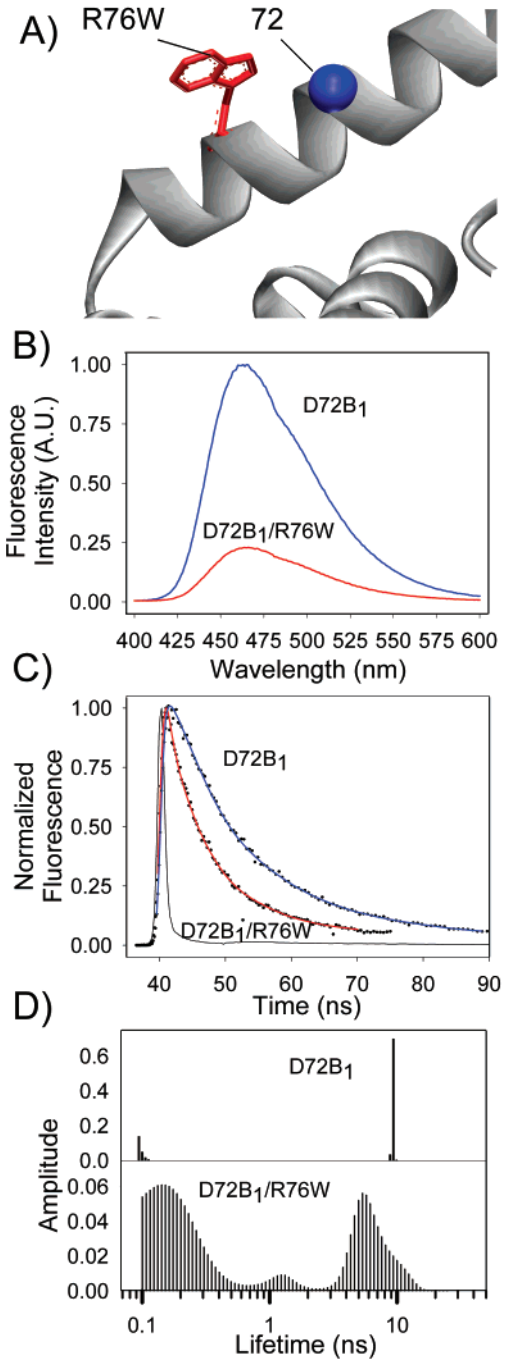

FIGURE 4: Location and fluorescence properties of bimane labels at site 72 before and after introducing a Trp residue one turn away at site 76. (A) Model of T4 lysozyme indicating α-carbon for site $D72B_1$ and R76W. (B) Fluorescence emission spectrum of $D72B_1$ and $D72B_1/R76W$. Notice the ~4× decrease in bimane fluorescence for the label at site 72 after a Trp residue is introduced at site 76. (C) Fluorescence decay of $D72B_1$ and $D72B_1/R76W$. (D) ESM analysis of mutants $D72B_1$ and $D72B_1/R76W$. Notice that the single lifetime for mutant $D72B_1$ is converted to a complex ESM pattern upon introducing the Trp residue at site 76.

to affect the protein stability compared to the previous single cysteine mutants (see Table 1). Note that the four sites in lysozyme being tested were previously shown (*9*) to have normal bimane fluorescence characteristics [i.e., quantum yields of ~0.2 or greater (see Figure 1B) and monoexponential fluorescence decay properties].

The Fluorescence Properties of the N116W Mutants Depend on the Distance of Bimane from N116W. The site-

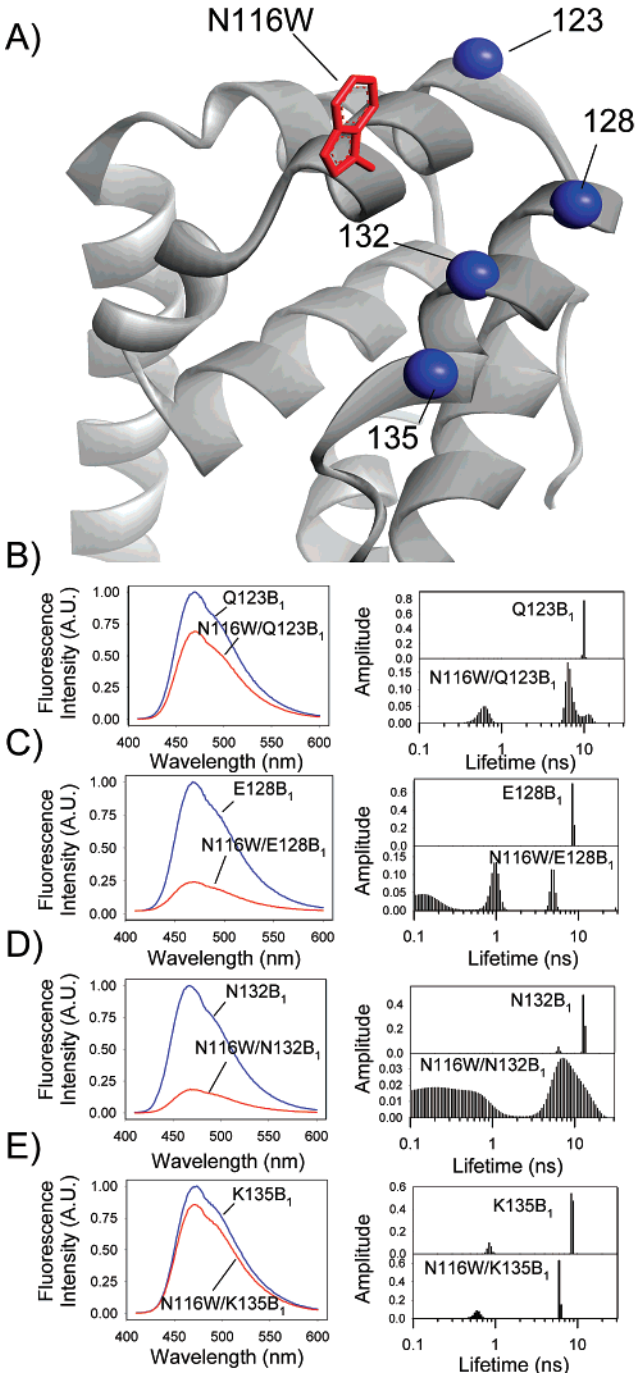

FIGURE 5: (A) Model of T4 lysozyme indicating the α-carbon site for each cysteine substitution and the location of the tryptophan residue introduced in this region (N116W). (Left panels, B−E) Steady-state fluorescence intensity measurements of mBBr-labeled cysteine mutants with and without the Trp residue introduced at site 116. Notice the decrease in fluorescence intensity, especially at sites 128 and 132, upon introduction of the Trp residue. (Right panels, B−E) ESM analyses of proteins in the presence and absence of the Trp residue at site 116. Note the low number of apparent lifetimes in the absence of the N116W residue (top half of each panel on the right side of the figure). This is in sharp contrast to the multiple species seen in the ESM decay analysis data for some of the same labeling sites containing the Trp residue at site 116 (bottom half of each panel on the right side of the figure).

specific effects of N116W on the neighboring bimane fluorescence intensity depend on the relative proximity to the bimane side chain (Table 1, left panels Figure 5B−E). What is more important, the distance dependence is in qualitative agreement with the crystal structure. For instance, the bimane label at site 132 shows the largest quenching, consistent with it being closest to the tryptophan at site 116 based on the structure. In contrast, bimane at site 135 is the farthest and shows the least quenching.

In addition to quenching the steady-state fluorescence intensity, the Trp residue introduced at N116W causes dramatic effects on the decay properties of some of the neighboring bimane labels. For example, the presence of the Trp residue at site 116 increases the fluorescence decay rates (shortens the fluorescence lifetime) for the bimane labels at sites 128 and 132 (Table 2). Not only are the decay rates faster but they are also more complicated, as can be seen graphically from analysis of the decay data using the ESM method for measuring lifetime distributions (right panels, Figure 5C,D). As found for the previous mutants, the ESM analysis of the bimane-labeled mutants without the Trp residue is essentially monoexponential (Figure 5B−E, top half of each panel on the right). However, the introduction of the Trp residue results in multiexponential decay characteristics for most of the sites, which is reflected in the distribution of lifetimes observed in the ESM analysis (Figure 5B−E, bottom half of each panel on the right).

DISCUSSION

The fluorescent probe monobromobimane is an excellent reporter group for protein structural studies. As a probe, it has a relatively small molar volume, and thus introduces minimal structural perturbation, and shows a defined solvent-dependent shift in its emission spectra (*8*, *9*).

However, we recently noticed several unusual aspects of bimane fluorescence during an SDFL study of T4 lysozyme: at a number of attachment sites on the protein, the bimane fluorescence intensity was abnormally low and the decay kinetics were complex (*9*). What was the cause of these anomalies? Closer analysis of the T4L crystal structure revealed that all of the anomalous bimane sites were close to a Trp residue, suggesting the tryptophans might be causing the abnormal bimane fluorescence. A search of the literature supported this theory; in a study of small, bimane-labeled peptides, Kosower and colleagues found that only Trp (and to a much lesser extent tyrosine) affected the bimane fluorescence (*23*).

Thus, we tested two of the affected sites (K124 and L133) to determine the effect of mutating the proximal tryptophan residues to a phenylalanine. In both cases the substitution caused an increase in bimane fluorescence intensity and a simplification of the fluorescence decay kinetics (Tables 1 and 2, Figures 2 and 3). Further, we found the reverse to be true: introducing a Trp residue (at site 76) caused quenching of a nearby bimane label (at site 72) one turn away on the same helix (Tables 1 and 2, Figure 4).

These observations are important for two reasons: they highlight an interesting property of bimane fluorescence, and they suggest a possible use of this phenomenon in protein structure−function studies. Although SDFL scans can yield information about secondary structural elements and the solvent-accessible surfaces of proteins, determining the three-dimensional arrangement (packing) of these elements is more difficult. The distance constraints provided by the Trp quenching of bimane might provide tertiary structure (pack-

ing) information to complement secondary structural information obtained from an SDFL scan.

With this goal in mind, we tested whether Trp quenching of bimane could be used to measure distance separations between sites in a protein, such as between two helices. We introduced the Trp residue at a location (site 116) that should cause different amounts of quenching of bimane labels attached to neighboring sites. As expected, the Trp mutation at site 116 caused variations in the fluorescence intensity/quantum yields from bimane labels at neighboring sites 123, 128, 132, and 135. The extent of the quenching was in qualitative agreement with the distance between the Trp residue and these sites on the T4L structure (compare Figure 5 with the data in Tables 1 and 2).

Probable Mechanism for Trp Quenching of Bimane Fluorescence. Why do the proximal Trp residues cause such dramatic quenching of bimane fluorescence? The probable cause of the quenching is through photoinduced electron transfer (PET) from Trp to the excited-state bimane. Bimane is sensitive to quenching by electron-donating groups (*39*, *43*), and the Trp quenching of bimane on peptides was proposed to occur by the Trp donating an electron to the excited-state bimane (*23*). We calculated the possible driving force for a PET process from Trp to bimane (using their E_{ox} and E_{red} values) and found it to be $\Delta G_{el} = -0.816$ eV, indicating an exergonic and thus likely process (see Materials and Methods). According to the PET fluorescence quenching hypothesis, after electron transfer from the Trp to the proximal bimane, the resulting radical ion pair, Trp ($+\cdot$): Bim($-\cdot$), would undergo reverse electron transfer to return the bimane to the ground state (S_0) in a radiationless manner.

Similarly, excited-state electron transfer has been ascribed to be the cause of tryptophan fluorescence and phosphorescence quenching (*44*, *45*) and be the cause of the complicated, multiexponential decay properties often observed for the tryptophan fluorescence in many proteins (*24*, *46*). The fluorescence decay data also support a PET fluorescence quenching mechanism. In every case tested, bimane residues most able to come within contact distance of a Trp residue showed shorter lifetimes in the two-exponential analysis and multiple lifetime species in the ESM analysis, whereas removing the neighboring Trp caused an increase in the lifetimes and a simplification of the ESM decay analysis.

Assuming a PET quenching mechanism, we calculated rate constants for the electron transfer from Trp to bimane (k_{ET}) for each of the mutants. These rates were calculated as described in Materials and Methods and are given in Table 3. The calculated k_{ET} rates (maximum value $\sim 5 \times 10^8$ s^{-1}) are in reasonable agreement with a PET mechanism. Note that both the changes in fluorescence lifetime and the changes in fluorescence intensity were used to calculate the k_{ET} rates. This approach avoids the possibility of missing very rapid PET occurring from proximal conformers that would be too fast to detect with our lifetime instrumentation, as it would still appear as a decrease in steady-state fluorescence intensity. Several instances where $k_{ET}^F > k_{ET}^\tau$ can be seen in Table 3.

In principle, it should be possible to use these k_{ET} rates, combined with the driving force for the PET, to determine distances between the Trp donor and bimane acceptor. Unfortunately, to accurately assess distances between the Trp and bimane pairs using the calculated k_{ET} rates is beyond the scope of the present work. Unknown variables in such calculations include uncertainty in the solvent polarity on protein surfaces (*47*), as well as distance, steric, and stereochemical factors (*48*) such as the shape and relative orientation of the two molecule pairs (*49*). Thus, instead of approximating distances from the k_{ET} rates, we propose a more simple, qualitative way to assess the proximity of Trp and bimane residues directly from the fluorescence data, described below.

Table 3: Electron Transfer Rates and Intensity and Lifetime Ratios Calculated from Trp Quenching of Bimane- Labeled Samples

bimane attachment site	$k_{ET}^{\tau\,a}$ ($\times 10^8$ s^{-1})	$k_{ET}^{F\,a}$ ($\times 10^8$ s^{-1})	ratio τ_0/τ_w [a,b]	ratio F_0/F_w [b]
124	3.8	4.8	4.5	5.5
133	1.7	4.8	2.2	4.2
72	1.4	3.3	2.4	4.2
123	0.7	0.5	1.6	1.5
128	3.7	3.1	4.0	3.7
132	0.7	4.0	1.8	5.3
135	0.6	0.3	1.4	1.2

[a] Electron transfer rates (k_{ET}) calculated as described in Materials and Methods using the fluorescence intensity (k_{ET}^F) and lifetime (k_{ET}^τ) measured with and without the proximal Trp residue. The lifetime values (τ) used were the weighted lifetimes assuming a biexponential distribution, defined by $f_1\tau_1 + f_2\tau_2$, where $f_1 = \alpha_1/(\alpha_1 + \alpha_2)$ and $f_2 = \alpha_2/(\alpha_1 + \alpha_2)$. [b] The ratio of the fluorescence values (intensity, F, and weighted lifetime, τ), without (F_0 and τ_0) and with (F_w and τ_w) the presence of the neighboring Trp residue, measured with 381 nm excitation, as described in Materials and Methods.

Simple, Qualitative Way To Classify the Different Types of Trp/Bimane Quenching. We propose that comparing the steady-state and fluorescence lifetime data provides a qualitative yet reliable assessment of the proximity of the Trp/bimane pair. In this approach, one first determines the ratio of the fluorescence intensity without (F_0) and with (F_w) the presence of the tryptophan residue (F_0/F_w) and then compares this value to the ratio obtained from the weighted fluorescence lifetime data without and with the Trp residue (τ_0/τ_w). Note that the weighted fluorescence lifetime data are proportional to the steady-state fluorescence intensity (*50*).

These ratios are then used to assess whether the Trp/bimane pair is "not close" (>15 Å), "close" (~10−15 Å), or "very close" (5−10 Å). Not close pairs are defined as those in which no effect of Trp on the bimane fluorescence is observed. Close pairs are those showing significant dynamic fluorescence quenching, i.e., quenching that occurs because the two species are able to collide during the lifetime of the bimane excited state. Dynamic quenching is indicated when both the steady-state fluorescence intensity and fluorescence lifetimes decrease by roughly the same amount (i.e., $F_0/F_w > 1$, $\tau_0/\tau_w > 1$, and $F_0/F_w \approx \tau_0/\tau_w$) (*51*).

We are defining very close Trp/bimane pairs to be pairs for which static fluorescence quenching is observed. Static quenching is indicated when the fluorescence intensity decreases but the fluorescence lifetimes do not change (i.e., $F_0/F_w > 1$, but $\tau_0/\tau_w \approx 1$) (*51*). Static quenching can occur only when two molecules are initially very close (i.e., within contact distance) at the moment of fluorophore excitation. At these close distances, the quenching occurs because the two molecules have either formed a ground-state, nonfluorescent complex or alternatively because they undergo a "dynamic" quenching process so rapid that it cannot be

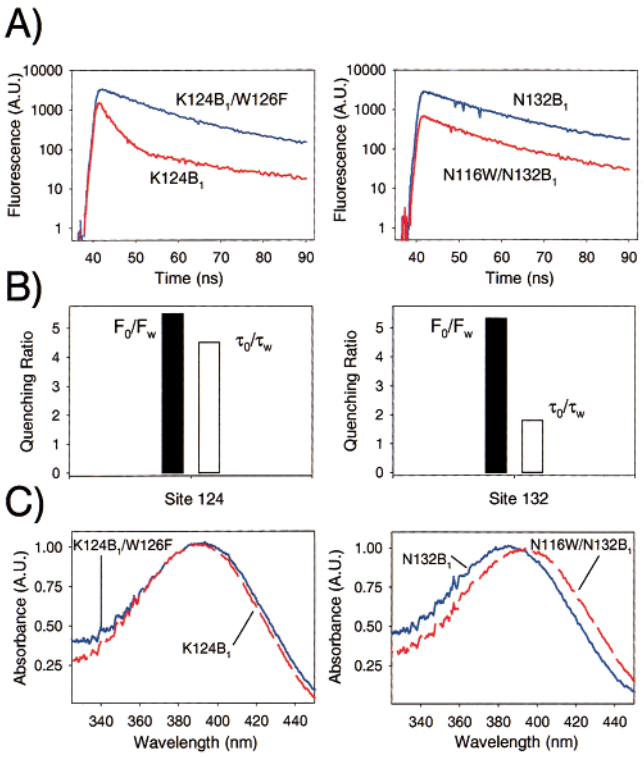

FIGURE 6: Fluorescence decay profiles and steady-state intensities indicate that some T4L mutants show dynamic quenching and others static quenching. (A) Fluorescence decay profiles of bimane at sites 124 and 132. The profiles are shown as log fluorescence intensity to more easily allow comparison. Notice that the decay at site 124 changes sharply in the presence of the Trp residue (suggesting a dynamic quenching mechanism), whereas the decays at site 132 show very similar rates (indicating the quenching occurs through a static-like mechanism). (B) Graph comparing the ratio of steady-state intensites (F_0/F_w) and fluorescence lifetimes (τ_0/τ_w). (C) Absorption spectra of bimane labels attached at sites 124 and 132 with (dashed line) and without (solid line) the presence of the neighboring Trp residue. Notice the change in the absorption spectra at site 132, suggesting a ground-state complex for mutant N116W/N132B_1.

detected by the fluorescence lifetime instrumentation (*52*).

The different intensity and lifetime ratios for the Trp/bimane mutants are given in Table 3. An example of dynamic vs static quenching for the T4L mutants is shown in Figure 6. Figure 6A shows the effect of the quenching phenomenon on the fluorescence lifetime decays, with the decay intensity plotted on a log scale. Note the rapid, sharp component to the decay of K124B_1 compared to K124B_1/W126F, indicating a dynamic quenching mechanism. In contrast, no such rapid component is observed in the decay of mutant N116W/N132B_1; rather the two decays are seen to be nearly parallel. These results suggest that at least some fraction of the Trp/bimane pair in N116W/N132B_1 is very close, forming a nonfluorescent ground-state complex or, alternatively, the PET-induced quenching is too fast to be resolved by our instrumentation.

Similarly, the bar graphs in Figure 6B compare the quenching ratios of the steady-state fluorescence intensity (F_0/F_w) with the quenching ratios determined from the weighted fluorescence lifetimes (τ_0/τ_w). As can be seen, the bimane at 124 shows dynamic quenching ($F_0/F_w \approx \tau_0/\tau_w$), whereas the bimane at 132 shows substantial static quenching ($F_0/F_w \gg \tau_0/\tau_w$), suggesting that the bimane at site 132 is very close to N116W and thus is being quenched by a static process. Note also that the absorption spectrum is altered for mutant N116W/N132B_1 compared to mutant N132B_1, also suggestive of a ground-state complex for the former mutant (Figure 6C). Note further that the same conclusions can be reached by comparing the ratio of the k_{ET}^F and k_{ET}^τ rates for each mutant.

Conclusion. We have shown that Trp quenching of bimane fluorescence can be used to measure proximity within proteins. The amount of quenching depends on the distance between the two molecules as well as on their ability to come within contact, and thus these constraints limit the number of Trp/bimane pairs that are able to show quenching. However, these limitations are also a strength of this method, since it is only sensitive to local, short-range interactions that are difficult to measure using longer range FRET methods. Another advantage of this method is that these short-range interactions can be measured using widely available fluorescence instrumentation and requires only minimal amounts of sample. More quantitative interpretations of distance constraints await further studies, including analysis of crystal structures of bimane-labeled samples combined with molecular modeling and analysis of the time-resolved data using the distance-dependent quenching model of Zelent et al. (*53*). Work of this type is currently underway in our laboratory. Because the Trp quenching of bimane is easily detected, we anticipate this phenomenon will be useful in protein folding studies, the detection of protein−protein interactions, and the monitoring of protein conformational changes.

ACKNOWLEDGMENT

We thank Dr. A. Beth for critical reading of the manuscript.

REFERENCES

1. Altenbach, C., Yang, K., Farrens, D. L., Farahbakhsh, Z. T., Khorana, H. G., and Hubbell, W. L. (1996) *Biochemistry 35*, 12470−12478.
2. McHaourab, H. S., Lietzow, M. A., Hideg, K., and Hubbell, W. L. (1996) *Biochemistry 35*, 7692−7704.
3. Farrens, D. L. (1999) in *Structure−Function Analysis of G Protein-Coupled Receptors* (Wess, J., Ed.) pp 289−314, Wiley-Liss, New York.
4. Hubbell, W. L., Cafiso, D. S., and Altenbach, C. (2000) *Nat. Struct. Biol. 7*, 735−739.
5. Flitsch, S. L., and Khorana, H. G. (1989) *Biochemistry 28*, 7800−7805.
6. Wu, J., and Kaback, H. R. (1994) *Biochemistry 33*, 12166−12171.
7. Barry, J. K., and Matthews, K. S. (1997) *Biochemistry 36*, 15632−15642.
8. Dunham, T. D., and Farrens, D. L. (1999) *J. Biol. Chem. 274*, 1683−1690.
9. Mansoor, S. E., McHaourab, H. S., and Farrens, D. L. (1999) *Biochemistry 38*, 16383−16393.
10. Shepard, L. A., Heuck, A. P., Hamman, B. D., Rossjohn, J., Parker, M. W., Ryan, K. R., Johnson, A. E., and Tweten, R. K. (1998) *Biochemistry 37*, 14563−14574.
11. Kachel, K., Ren, J., Collier, R. J., and London, E. (1998) *J. Biol. Chem. 273*, 22950−22956.
12. Sinev, M. A., Sineva, E. V., Ittah, V., and Haas, E. (1996) *Biochemistry 35*, 6425−6437.
13. Navon, A., Ittah, V., Landsman, P., Scheraga, H. A., and Haas, E. (2001) *Biochemistry 40*, 105−118.
14. Cha, A., Snyder, G. E., Selvin, P. R., and Bezanilla, F. (1999) *Nature 402*, 809−813.

15. Yang, C. S., Skiba, N. P., Mazzoni, M. R., and Hamm, H. E. (1999) *J. Biol. Chem. 274*, 2379−2385.
16. McHaourab, H. S., Oh, K. J., Fang, C. J., and Hubbell, W. L. (1997) *Biochemistry 36*, 307−316.
17. Koteiche, H. A., and McHaourab, H. S. (1999) *J. Mol. Biol. 294*, 561−577.
18. Farrens, D. L., Altenbach, C., Yang, K., Hubbell, W. L., and Khorana, H. G. (1996) *Science 274*, 768−770.
19. Perozo, E., Cortes, D. M., and Cuello, L. G. (1998) *Nat. Struct. Biol. 5*, 459−469.
20. Rabenstein, M. D., and Shin, Y. K. (1996) *Biochemistry 35*, 13922−13928.
21. Yuan, T., Weljie, A. M., and Vogel, H. J. (1998) *Biochemistry 37*, 3187−3195.
22. Ghanouni, P., Steenhuis, J. J., Farrens, D. L., and Kobilka, B. K. (2001) *Proc. Natl. Acad. Sci. U.S.A. 98*, 5997−6002.
23. Sato, E., Sakashita, M., Kanaoka, Y., and Kosower, E. M. (1988) *Bioorg. Chem. 16*, 298−306.
24. Hudson, B. S. (1999) *Acc. Chem. Res. 32*, 297−300.
25. Matsumura, M., and Matthews, B. W. (1989) *Science 243*, 792−794.
26. Ho, S. N., Hunt, H. D., Horton, R. M., Pullen, J. K., and Pease, L. R. (1989) *Gene 77*, 51−59.
27. Sauer, U. H., San, D. P., and Matthews, B. W. (1992) *J. Biol. Chem. 267*, 2393−2399.
28. Inoue, H., Nojima, H., and Okayama, H. (1990) *Gene 96*, 23−28.
29. Eftink, M. R. (1994) *Biophys. J. 66*, 482−501.
30. Pace, C. N., and Scholtz, J. M. (1997) in *Protein Structure: A Practical Approach* (Creighton, T. E., Ed.) Chapter 12, Oxford University Press, New York.
31. Novokhatny, V., Medved, L., Mazar, A., Marcotte, P., Henkin, J., and Ingham, K. (1992) *J. Biol. Chem. 267*, 3878−3885.
32. Becktel, W. J., and Schellman, J. A. (1987) *Biopolymers 26*, 1859−1877.
33. Ware, W. R., Doemeny, L. J., and Nemzek, T. L. (1973) *J. Phys. Chem. 77*, 2038−2048.
34. O'Connor, D., and Phillips, D. (1984) *Time Correlated Single Photon Counting*, Academic Press, San Diego, CA.
35. Holzwarth, A. R. (1995) *Methods Enzymol. 246*, 334−362.
36. Rehm, D., and Weller, A. (1970) *Isr. J. Chem. 8*, 259.
37. Kavarnos, G. J. (1990) in *Photoinduced Electron Transfer I* (Mattay, J., Ed.) pp 23−58, Springer-Verlag, Berlin.
38. Kavarnos, G. J. (1993) *Fundamentals of Photoinduced Electron Transfer*, VCH Publishers, New York, NY.
39. Kosower, E. M., Kanety, H., Dodluk, H., and Hermolin, J. (1982) *J. Phys. Chem. 86*, 1270−1277.
40. Jones, G. I., Farahat, C. W., and Oh, C. (1994) *J. Phys. Chem. 98*, 6906−6909.
41. Williams, R. M., Zwier, J. J., and Verhoeven, J. W. (1995) *J. Am. Chem. Soc. 117*, 4093−4099.
42. Matthews, B. W. (1995) *Adv. Protein Chem. 46*, 249−278.
43. Kosower, E. M., Giniger, R., Radkowsky, A., Hebel, D., and Shusterman, A. (1986) *J. Phys. Chem. 90*, 5552−5557.
44. Eftink, M. R. (1991) in *Topics in Fluorescence Spectroscopy* (Lakowicz, J. R., Ed.) pp 53−126, Plenum Press, New York.
45. Vanderkooi, J. M., Englander, S. W., Papp, S., Wright, W. W., and Owen, C. S. (1990) *Proc. Natl. Acad. Sci. U.S.A. 87*, 5099−5103.
46. Chen, Y., and Barkley, M. D. (1998) *Biochemistry 37*, 9976−9982.
47. Lockhart, D. J., and Kim, P. S. (1992) *Science 257*, 947−951.
48. Closs, G. L., and Miller, J. R. (1988) *Science 240*, 440−447.
49. Siders, P., Cave, R. J., and Marcus, R. A. (1984) *J. Chem. Phys. 81*, 5613−5624.
50. Lakowicz, J. R. (1999) *Principles of fluorescence spectroscopy*, 2nd ed., Kluwer Academic/Plenum, New York.
51. Lakowicz, J. R., and Weber, G. (1973) *Biochemistry 12*, 4161−4170.
52. Webber, S. E. (1997) *Photochem. Photobiol. 65*, 33−38.
53. Zelent, B., Kusba, J., Gryczynski, I., Johnson, M. L., and Lakowicz, J. R. (1998) *Biophys. Chem. 73*, 53−75.

BI011198I